MITSUBISHI ELECTRIC RESEARCH LABORATORIES
http://www.merl.com

SEAGLE: Robust Computational Imaging under Multiple Scattering

Liu, H.-Y.; Liu, D.; Mansour, H.; Boufounos, P.T.; Waller, L.; Kamilov, U.

TR2017-081 June 2017

Abstract

Multiple scattering of light as it passes through an object is a fundamental problem limiting the performance of imaging systems. We describe a new technique for robust imaging under multiple scattering based on a nonlinear scattering model and sparse-regularization.

OSA Imaging and Applied Optics Congress

SEAGLE: Robust Computational Imaging under Multiple Scattering

H.-Y. Liu[1], D. Liu[2], H. Mansour[2], P. T. Boufounos[2], L. Waller[1], and U. S. Kamilov[2,*]

[1]*Department of Electrical Engineering and Computer Sciences, University of California, Berkley, CA, USA*
[2]*Mitsubishi Electric Research Laboratories (MERL), Cambridge, MA, USA.*

[*]*Email:* kamilov@merl.com.

Abstract: Multiple scattering of light as it passes through an object is a fundamental problem limiting the performance of imaging systems. We describe a new technique for robust imaging under multiple scattering based on a nonlinear scattering model and sparse-regularization.

OCIS codes: (110.1758) Computational Imaging; (290.4210) Multiple Scattering; (100.3200) Inverse Scattering.

1. Introduction

Estimation of the spatial permittivity distribution of an unknown object from the measurements of the scattered light-field is common in numerous imaging applications such as tomographic microscopy [1] and digital holography [2]. Traditionally, this inverse scattering problem is approximately solved by linearizing the relationship between the permittivity distribution and the measured light. A linear forward model can be obtained by assuming a straight-ray propagation of light, or by adopting more refined scattering models based on the first Born or Rytov approximations [3].

Linear scattering models assume weakly scattering objects, making corresponding imaging methods inherently inaccurate for many applications. This places fundamental limits—in terms of resolution, penetration, and quality—on the imaging systems relying on such models. Increasingly, however, inverse scattering approaches are being formulated as large-scale optimization problems, combining nonlinear scattering models with regularizers that can increase the robustness to noise and limited-data artifacts [4–7]. In this paper, we discuss an extension of the prior work by a new nonlinear scattering model and a total variation (TV) regularized inversion algorithm [8]. The key aspect of the proposed method—called Series Expansion with Accelerated Gradient Descent on Lippmann-Schwinger Equation (SEAGLE)—is its efficiency and stability, even for objects with large permittivity contrasts. This makes it suitable for robust imaging under multiple scattering. Here, we experimentally validated SEAGLE on the dataset [9], which contains measurements of strongly scattering objects at microwave frequencies.

2. Method

Consider the scattering problem (Fig. 1) where an object of the permittivity distribution $\varepsilon(\boldsymbol{x})$ in the bounded domain Ω is immersed into a background medium of permittivity ε_b and illuminated with the incident electric field $u_{\text{in}}(\boldsymbol{x})$. We assume that the incident field is monochromatic and coherent, and it is known inside Ω and at the locations of the sensors. The result of object-light interaction is measured at the location of the sensors as a scattered field $u_{\text{sc}}(\boldsymbol{x})$. The

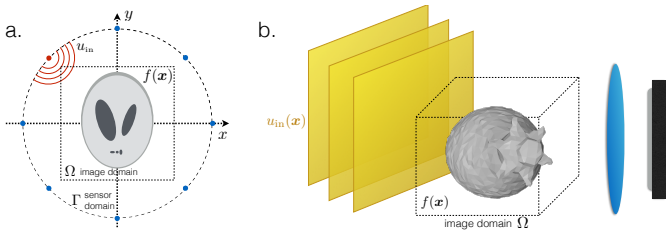

Fig. 1. Schematic representation of scattering scenarios in two and three dimensions. An object of a scattering potential $f(\boldsymbol{x})$ is illuminated with an input wave u_{in}, which interacts with the object and leads to the scattered wave u_{sc} at the sensors.

multiple scattering of light can be accurately described by the Lippmann-Schwinger equation inside the image domain

$$u(\boldsymbol{x}) = u_{\text{in}}(\boldsymbol{x}) + \int_{\Omega} g(\boldsymbol{x}-\boldsymbol{x}')\, f(\boldsymbol{x}')\, u(\boldsymbol{x}')\, \mathrm{d}\boldsymbol{x}', \quad (\boldsymbol{x} \in \Omega) \tag{1}$$

where $u(\boldsymbol{x}) = u_{\text{in}}(\boldsymbol{x}) + u_{\text{sc}}(\boldsymbol{x})$ is the total electric field, $f(\boldsymbol{x}) \triangleq k^2(\varepsilon(\boldsymbol{x}) - \varepsilon_b)$ is the scattering potential, which is assumed to be real, and $k = 2\pi/\lambda$ is the wavenumber in vacuum. The function $g(\boldsymbol{x})$ is the Green's function defined as

$$g(\boldsymbol{x}) \triangleq \begin{cases} \dfrac{\mathrm{j}}{4} H_0^{(1)}(k_b \|\boldsymbol{x}\|_{\ell_2}) & \text{in 2D} \\ \dfrac{\mathrm{e}^{\mathrm{j}k_b\|\boldsymbol{x}\|_{\ell_2}}}{4\pi\|\boldsymbol{x}\|_{\ell_2}} & \text{in 3D,} \end{cases} \tag{2}$$

where $k_b \triangleq k\sqrt{\varepsilon_b}$ is the wavenumber of background medium and $H_0^{(1)}$ is the zero-order Hankel function of the first kind. Note that the knowledge of the total-field u inside the image domain Ω enables the prediction of the scattered field at the sensor domain

$$u_{\text{sc}}(\boldsymbol{x}) = \int_{\Omega} g(\boldsymbol{x}-\boldsymbol{x}')\, f(\boldsymbol{x}')\, u(\boldsymbol{x}')\, \mathrm{d}\boldsymbol{x}'. \quad (\boldsymbol{x} \in \Gamma) \tag{3}$$

The discretization and combination of (1) and (3) leads to the following matrix-vector description of the scattering problem

$$\mathbf{y} = \mathbf{H}(\mathbf{u} \bullet \mathbf{f}) + \mathbf{e} \tag{4a}$$

$$\mathbf{u} = \mathbf{u}_{\text{in}} + \mathbf{G}(\mathbf{u} \bullet \mathbf{f}), \tag{4b}$$

where $\mathbf{f} \in \mathbb{R}^N$ is the discretized scattering potential f, $\mathbf{y} \in \mathbb{C}^M$ is the measured scattered field u_{sc} at Γ, $\mathbf{u}_{\text{in}} \in \mathbb{C}^N$ is the input field u_{in} inside Ω, $\mathbf{H} \in \mathbb{C}^{M\times N}$ is the discretization of the Green's function at Γ, $\mathbf{G} \in \mathbb{C}^{N\times N}$ is the discretization of the Green's function inside Ω, $\bullet$ denotes a component-wise multiplication between two vectors, and $\mathbf{e} \in \mathbb{C}^M$ models the random noise at the measurements. Using the shorthand notation $\mathbf{A} \triangleq \mathbf{I} - \mathbf{G}\mathrm{diag}\{\mathbf{f}\}$, where $\mathbf{I} \in \mathbb{R}^{N\times N}$ is the identity matrix and $\mathrm{diag}\{\cdot\}$ is an operator that forms a diagonal matrix from its argument, we can represent the forward scattering in (4b) as a minimization problem

$$\widehat{\mathbf{u}}(\mathbf{f}) \triangleq \underset{\mathbf{u}\in\mathbb{C}^N}{\arg\min}\, \{\mathscr{S}(\mathbf{u})\} \quad \text{with} \quad \mathscr{S}(\mathbf{u}) \triangleq \frac{1}{2}\|\mathbf{A}\mathbf{u} - \mathbf{u}_{\text{in}}\|_{\ell_2}^2. \tag{5}$$

The gradient of $\mathscr{S}$ can be computed as $\nabla\mathscr{S}(\mathbf{u}) = \mathbf{A}^{\mathrm{H}}(\mathbf{A}\mathbf{u} - \mathbf{u}_{\text{in}})$, which allows us to compute the total field $\widehat{\mathbf{u}}$ iteratively using the Nesterov's accelerated gradient method [10]

$$q_t \leftarrow \frac{1}{2}\left(1 + \sqrt{1 + q_{t-1}^2}\right) \tag{6a}$$

$$\mathbf{s}^t \leftarrow \mathbf{u}^t + ((q_{t-1} - 1)/q_t)(\mathbf{u}^t - \mathbf{u}^{t-1}) \tag{6b}$$

$$\mathbf{u}^t \leftarrow \mathbf{s}^t - \nu\mathbf{A}^{\mathrm{H}}(\mathbf{A}\mathbf{s}^t - \mathbf{u}_{\text{in}}), \tag{6c}$$

for $t = 1, 2, \ldots, T$, where $\mathbf{u}^{-1} = \mathbf{u}^0 = \mathbf{u}_{\text{in}}$, $q_0 = 1$, and $\nu > 0$ is the step-size. We finally set the predicted scattered field to $\mathbf{z}(\mathbf{f}) = \mathbf{H}(\widehat{\mathbf{u}}(\mathbf{f}) \bullet \mathbf{f})$ with $\widehat{\mathbf{u}}(\mathbf{f}) = \mathbf{u}^T$.

It is worth noting that the final $\mathbf{z}$ returned by our forward scattering model is a function of $\mathbf{f}$, which leads to the following formulation of the inverse scattering problem

$$\widehat{\mathbf{f}} = \underset{\mathbf{f}\in\mathbb{C}^N}{\arg\min}\, \{\mathscr{D}(\mathbf{f}) + \mathscr{R}(\mathbf{f})\}, \tag{7}$$

where

$$\mathscr{D}(\mathbf{f}) \triangleq \frac{1}{2}\|\mathbf{y} - \mathbf{z}(\mathbf{f})\|_{\ell_2}^2 \quad \text{and} \quad \mathscr{R}(\mathbf{f}) \triangleq \tau \sum_{n=1}^{N} \|[\mathbf{D}\mathbf{f}]_n\|_{\ell_2}. \tag{8}$$

Here, $\mathscr{D}$ is the data-fidelity term that measures the discrepancy between the actual measurements $\mathbf{y}$ and the ones predicted by our scattering model $\mathbf{z}$. The functional $\mathscr{R}$ is the isotropic TV regularizer with the parameter $\tau > 0$ controlling

the strength of the regularization. The image formation can then be done iteratively, using the proximal-gradient method

$$\mathbf{f}^i \leftarrow \text{prox}_{\gamma\mathscr{R}}\left(\mathbf{f}^{i-1} - \gamma\nabla\mathscr{D}(\mathbf{f}^{i-1})\right), \tag{9}$$

for $i = 1,2,3,\ldots$, where $\gamma > 0$ is a step-size. The operator $\text{prox}_{\gamma\mathscr{R}}$ for isotropic TV can be efficiently evaluated [11]. The gradient is given by $\nabla\mathscr{D}(\mathbf{f}) = \text{Re}\{\mathbf{r}^0\}$, where $\mathbf{r}^0$ is computed using the following iteration

$$\mathbf{T}^t \leftarrow \text{diag}\left\{\mathbf{G}^{\text{H}}(\mathbf{A}\mathbf{s}^t - \mathbf{u}_{\text{in}})\right\}^{\text{H}} + \text{diag}\{\mathbf{s}^t\}^{\text{H}}\mathbf{G}^{\text{H}}\mathbf{A} \tag{10a}$$

$$\mathbf{q}^{t-1} \leftarrow (1-\mu_t)\mathbf{S}\mathbf{q}^t + \mu_{t+1}\mathbf{S}\mathbf{q}^{t+1} \tag{10b}$$

$$\mathbf{r}^{t-1} \leftarrow \mathbf{r}^t + \nu\mathbf{T}^t\mathbf{q}^t, \tag{10c}$$

for $t = T, T-1, \ldots, 1$, where $\mathbf{s}^t$ is from (6b), $\mathbf{q}^{T+1} = 0$, $\mathbf{q}^T = \text{diag}\{\mathbf{f}\}^{\text{H}}\mathbf{H}^{\text{H}}(\mathbf{z}-\mathbf{y})$ and $\mathbf{r}^T = \text{diag}\{\widehat{\mathbf{u}}\}^{\text{H}}\mathbf{H}^{\text{H}}(\mathbf{z}-\mathbf{y})$. Here, we use the definitions $\mathbf{S} \triangleq \mathbf{I} - \nu\mathbf{A}^{\text{H}}\mathbf{A}$ and $\mu_t \triangleq (1-q_{t-1})/q_t$. The remarkable aspect of this backpropagation algorithm is that it allows for an explicit differentiation of a nonlinear scattering model with respect to the scattering potential, which in turn enables efficient large-scale computational imaging.

3. Results

To validate the algorithm, we consider experimental measuremnts of the object *FoamDielExtTM* from a dataset [9]. The object consists of two cylinders on a rim of radius of 1.67 m, and a measurement set-up is similar to that in Fig. 1(a). The image domain has size 15 cm $\times$ 15 cm. There are 9 transmitters and 240 detectors for each transmitter, all equally spaced on the rim. Our results in Fig. 2 use the data only at 3 GHz, and highlight the remarkable performance of SEAGLE on this strongly scattering object.

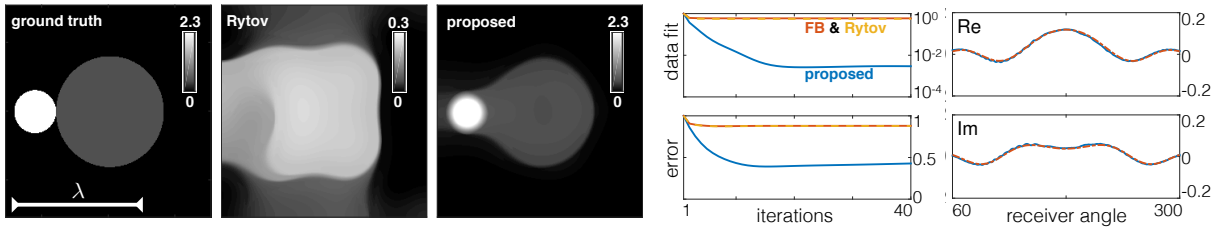

Fig. 2. Experimental validation of the proposed method on the highly scattering object *FoamDielExtTM*. The first three columns show from left to right, the ground truth, reconstruction using the Rytov approximation, and using SEAGLE, respectively. The fourth column shows the evolution of the normalized data-fit (top) and the normalized reconstruction error (bottom). The last column shows the true and predicted measurements for the transmission angle zero. The scale bar is equal to the wavelength λ at 3 GHz.

References

1. W. Choi, C. Fang-Yen, K. Badizadegan, S. Oh, N. Lue, R. R. Dasari, and M. S. Feld, "Tomographic phase microscopy," *Nat. Methods*, vol. 4, pp. 717–719, September 2007.
2. D. J. Brady, K. Choi, D. L. Marks, R. Horisaki, and S. Lim, "Compressive holography," *Opt. Express*, vol. 17, no. 15, pp. 13040–13049, 2009.
3. A. C. Kak and M. Slaney, *Principles of Computerized Tomographic Imaging*. IEEE, 1988.
4. L. Tian and L. Waller, "3D intensity and phase imaging from light field measurements in an LED array microscope," *Optica*, vol. 2, pp. 104–111, 2015.
5. U. S. Kamilov, I. N. Papadopoulos, M. H. Shoreh, A. Goy, C. Vonesch, M. Unser, and D. Psaltis, "Learning approach to optical tomography," *Optica*, vol. 2, pp. 517–522, June 2015.
6. T. Zhang, C. Godavarthi, P. C. Chaumet, G. Maire, H. Giovannini, A. Talneau, M. Allain, K. Belkebir, and A. Sentenac, "Far-field diffraction microscopy at $\lambda/10$ resolution," *Optica*, vol. 3, pp. 609–612, June 2016.
7. U. S. Kamilov, D. Liu, H. Mansour, and P. T. Boufounos, "A recursive Born approach to nonlinear inverse scattering," *IEEE Signal Process. Lett.*, vol. 23, pp. 1052–1056, August 2016.
8. H.-Y. Liu, U. S. Kamilov, D. Liu, H. Mansour, and P. T. Boufounos, "Compressive imaging with iterative forward models," in *Proc. IEEE Int. Conf. Acoustics, Speech and Signal Process. (ICASSP 2017)*, (New Orleans, LA, USA), March 5-9, 2017.
9. J.-M. Geffrin, P. Sabouroux, and C. Eyraud, "Free space experimental scattering database continuation: experimental set-up and measurement precision," *Inv. Probl.*, vol. 21, no. 6, pp. S117–S130, 2005.
10. Y. E. Nesterov, "A method for solving the convex programming problem with convergence rate $O(1/k^2)$," *Dokl. Akad. Nauk SSSR*, vol. 269, pp. 543–547, 1983. (in Russian).
11. A. Beck and M. Teboulle, "Fast gradient-based algorithm for constrained total variation image denoising and deblurring problems," *IEEE Trans. Image Process.*, vol. 18, pp. 2419–2434, November 2009.